Research Article

Synthesis dynamics of silver nanowires galvanically displaced by platinum salts: a fabrication route for oxygen reduction electrocatalysts and metal electrodeposition electrodes

Joseph F. Jeanetta[1] · Meagan M. LeBerth[1] · Darren D. Miller[1] · Christopher J. Barile[1]

Received: 31 March 2020 / Accepted: 12 June 2020 / Published online: 19 June 2020

Abstract
The advancement of conductive and flexible thin films is relevant to an assortment of energy applications ranging from organic photovoltaics, fuel cells, lithium ion batteries, and dynamic windows. Here, we develop an inexpensive, fast, and adjustable method to yield nanowire arrays on flexible polyethylene terephthalate substrates for the alkaline oxygen reduction reaction and for reversible metal electrodeposition. Ag nanowires serve as a non-sacrificial template for Pt deposition and allow for the synthesis of bimetallic Pt/Ag nanowires. When not properly controlled, the galvanic displacement reaction occurring at the solid–liquid interface between Ag nanowires and aqueous Pt ions results in nonuniform nucleation and growth profiles, which creates micron-sized gaps in the nanowire arrays. These gaps, which result in poorly conducting thin films, increase in prevalence when immersion length and Pt concentration are increased. Multiple cycles of 10-min immersions in 10 mM K_2PtCl_4 yield bimetallic Pt/Ag nanowires that maintain the high aspect ratios and conductivities of the initial Ag nanowires, while the added Pt improves electrocatalytic performance and electrochemical durability.

Keywords Platinum nanowires · Silver nanowires · Galvanic displacement · Oxygen reduction reaction · Electrocatalysis · Reversible metal electrodeposition

1 Introduction

Thin film electrodes are important in a number of renewable energy technologies including organic photovoltaics [1–3], polymer electrolyte membrane fuel cells [4], lithium ion batteries [5, 6], and dynamic windows [7]. There is an increasing demand for durable and affordable thin film transparent conductive electrodes (TCEs) for the aforementioned energy applications as well as for thin film transistors used in displays and touch screen devices [8, 9]. Tin-doped indium oxide (ITO) is currently the industrially preferred material for many TCE applications. However, there are several issues associated with ITO including its brittleness, chemical sensitivity, and high price due to the expense of sputter deposition and the limited global supply of In [10–13]. Therefore, researchers are developing novel transparent conductive materials that are more durable, flexible, and affordable. Emerging materials to replace ITO include carbon nanotubes [14], graphene [15], metallic nanowires [16, 17], and conductive polymers [18].

Of the metallic nanowires, thin films of silver nanowires (AgNWs) compete with ITO in transmittance and conductivity and outperform ITO in terms of flexibility [19]. The raw price of Ag and In are comparable, but AgNWs can be deposited by more affordable methods, such as spin coating [20], spray coating [21], electrodepostion [22], or roll-to-roll processing [23]. AgNWs have demonstrated good stability under several accelerated aging processes [24], however Ag is vulnerable to deterioration by oxidation and/or sulfidation when exposed to air [25]. Furthermore,

✉ Christopher J. Barile, cbarile@unr.edu | [1]Department of Chemistry, University of Nevada, Reno, NV 89557, USA.

the electrochemical window of AgNW electrodes is limited by the electrodissolution of Ag to Ag^+.

The aim of this manuscript is to contribute to the development of more stable thin film nanowire electrodes for electrochemical applications. We use a non-sacrificial template of AgNWs to synthesize thin conductive films of bimetallic Pt/AgNWs through a galvanic displacement reaction. Pt is an important electrocatalyst for many reactions including oxygen reduction, oxygen evolution, and carbon monoxide oxidation. These reactions are instrumental to proton exchange membrane fuel cells, rechargeable lithium-air batteries, and catalytic converters [26–29]. Additionally, Pt is one of the most inert metals, making Pt-based nanostructures good candidates for electrochemically stable thin film electrodes. However, the high cost of Pt and its compounds remains a challenge for industrial relevance. The need for affordable methods to synthesize Pt nanostructures motivates this work.

Galvanic displacement of AgNWs by chloroplatinic acid (H_2PtCl_6) was previously studied by Tan et al. In this work, AgNWs were used as a sacrificial template to yield porous Pt nanowires (PtNWs) by reacting AgNWs and H_2PtCl_6 in refluxing ethylene glycol [30]. However, the small scale of this synthesis route is problematic for deposition techniques producing conductive thin films, as the final PtNW product is very dilute. After considering the challenges associated with solution-phase PtNW synthesis, we hypothesized that conducting the galvanic displacement reaction at the solid–liquid interface would increase the usable Pt/AgNW yield. Specifically, substrates spin-coated with AgNWs would be immersed in solutions of Pt salts. Ideally, this process would both increase the scalability of production and result in Pt/AgNWs that maintain the high aspect ratios of the AgNW precursors.

In this manuscript, we systematically evaluate several synthesis conditions for the galvanic displacement of AgNWs by chloride-containing Pt species at the solid–liquid interface. Among other factors, we compared the effect of the oxidation state of Pt (4+ and 2+) on synthesis dynamics. The galvanic displacement reaction for $PtCl_6^{2-}$ reducing to solid $Pt_{(s)}$ occurs according to Eqs. (1) and (2), in which elemental Ag is oxidized to either $AgCl_{(s)}$ or $Ag^+_{(aq)}$, respectively. For $PtCl_4^{2-}$, the oxidation of the AgNWs to $AgCl_{(s)}$ crystals is thermodynamically spontaneous (Eq. 3), while the oxidation of elemental Ag to $Ag^+_{(aq)}$ is non-spontaneous (Eq. 4).

$$4Ag_{(s)} + PtCl_{6\ (aq)}^{2-} \rightarrow Pt_{(s)} + 4AgCl_{(s)} + 2Cl^-_{(aq)} + 1.262\ V \quad (1)$$

$$4Ag_{(s)} + PtCl_{6\ (aq)}^{2-} \rightarrow Pt_{(s)} + 4Ag^+_{(aq)} + 6\ Cl^-_{(aq)} + 0.684\ V \quad (2)$$

$$2Ag_{(s)} + PtCl_{4\ (aq)}^{2-} \rightarrow Pt_{(s)} + 2AgCl_{(s)} + 2\ Cl^-_{(aq)} + 0.536\ V \quad (3)$$

$$2Ag_{(s)} + PtCl_{4\ (aq)}^{2-} \rightarrow Pt_{(s)} + 2Ag^+_{(aq)} + 2\ Cl^-_{(aq)} - 0.042\ V \quad (4)$$

The above equations are important thermodynamic considerations for Pt/AgNWs synthesis. In addition to thermodynamic effects, we demonstrate that other parameters such as nucleation and growth dynamics affect reaction kinetics. Together, these attributes dictate the structure, composition, and electrochemical properties of the resulting Pt/AgNWs. We demonstrate that these Pt/AgNWs have applications as oxygen reduction electrocatalysts and reversible metal electrodeposition electrodes. We note that the described nanowire thin films are not highly transparent, and although it is possible to synthesize transparent conducting versions of the Pt/AgNWs, transparency is not a focus of this manuscript.

2 Materials and methods

Thin films of AgNWs were prepared by spin coating commercially obtained ~ 1% by mass AgNWs (diameter: 25–35 nm, length: 9–15 µm, CheapTubes, Inc.) in isopropanol onto 2 cm × 2 cm polyethylene terephthalate (PET) substrates. After 5 min of sonication, the AgNWs were deposited using a Laurell Technologies Model WS-400B-6NPP/LITE spin coater. The commercial AgNW solution (100 µL) was spun at 1000 rpm for 30 s with an acceleration of 10 rpm/s. The samples were then immersed in aqueous solutions of H_2PtCl_6 (Sigma Aldrich) or potassium tetrachloroplatinate (K_2PtCl_4) (Sigma Aldrich), dried under a stream of air, and then submerged in 100 mM ammonium hydroxide (NH_4OH). For experiments with Pt reactant concentrations varying between 10 mM and 100 µM, each solution contained the same number of moles (100 µmols). The 10 µM solution contained 10 µmols of Pt reactant. Sheet resistance measurements were conducted using a universal four-point probe instrument connected to a Jandel RM3 Test Unit. Mass measurements were made with a Sartorius analytical balance with a precision of 10 µg. Scanning electron microscope (SEM) images and energy-dispersive X-ray spectroscopy (EDX) data were obtained using a JOEL JSM-6010LA microscope with a working voltage of 10–20 kV. All Pt atomic percentages were calculated from the EDX spectra and are reported as compared to the total amount of Pt, Ag, and Cl. For experiments in which Pt atomic percentages were confirmed using inductively coupled plasma-mass spectrometry (ICP-MS), this technique was conducted by the Western Environmental Testing Laboratory (Sparks, NV).

For both sheet resistance measurements and Pt atomic percentage values, the values reported are averages across 2–4 samples measured at 5 different locations per sample. Errors bars reported represent standard deviations. UV–Vis spectroscopy analysis was conducted using a Shimadzu UV-2550 UV–Vis spectrophotometer. Electrochemical experiments were performed using a VSP-300 Biologic potentiostat. O_2 reduction reaction experiments were conducted in O_2-sparged 100 mM $KOH_{(aq)}$ using a Ag/AgCl (3 M KCl) reference electrode (eDaq, Inc.) and a Pt wire counter electrode. Reversible metal electrodeposition durability experiments were conducted by cyclic voltammograms from +0.8 to −0.6 V (vs. Ag/AgCl, Pt wire counter electrode) in an acidic (pH 2) Bi–Cu electrolyte. Various nanowire substrates were used as the working electrode with a 0.242 cm^2 geometric area. Commercial Pt nanowires were obtained from Metrohm USA (diameter: 150–250 nm, length: 10–16 µm).

3 Results and discussion

3.1 Understanding the galvanic displacement reaction of AgNWs by Pt

Thin films of AgNWs prepared by four successive spin coats were immersed in 100 µM H_2PtCl_6 or K_2PtCl_4. The volume of the solution was 1.0 L in order for the reaction to not be limited by Pt. Samples were immersed for 10, 30, 60, and 120 min on flexible 2 cm × 2 cm PET substrates. Ideally, the cation in both sets of experiments would be the same. However, the low solubility of potassium hexachloroplatinate (K_2PtCl_6) in water prevented us from studying it [31]. Likewise, the acidic Pt^{2+} analog, H_2PtCl_4, does not exist in the solid state [32].

Increases in sheet resistance (Fig. 1a) and atomic Pt percent (Fig. 1b) were observed as the duration of the immersion increased. Samples submerged in H_2PtCl_6 (Fig. 1, black) showed both a larger increase in sheet resistance and contained more Pt as determined by EDX than K_2PtCl_4 samples (Fig. 1, red). The measured sheet resistances of the Pt-modified AgNWs were orders of magnitude larger than the calculated theoretical sheet resistance. If the initial AgNWs (~ 2 Ω/sq) were replaced by structurally identical Pt nanowires, then the sheet resistance of the sample would increase ~ 7 times, to a sheet resistance of ~ 14 Ω/sq, because bulk Pt is about 7 times more resistive than bulk Ag [33]. The experimental sheet resistances of the Pt-modified AgNWs far exceed the theoretical ~ 14 Ω/sq value even when the Pt compositions are less than 100%, fit can therefore be concluded that other structural and/or chemical changes are occurring within the thin film.

SEM analysis showed that as the films of AgNWs underwent galvanic displacement by Pt, the nanowires became progressively thinner and formed an increasing number of gaps within the array as the reaction time elongated. Prior to immersion, the AgNWs are relatively homogenous, as shown in Fig. 2. After immersion in H_2PtCl_6 (Fig. 3) or K_2PtCl_4 (Fig. 4), holes within the array formed, resulting in an increased contrast between topographical regions. The holes within the nanowire array occur earlier and are larger for the samples immersed in H_2PtCl_6. The prevalence of these holes explains why the H_2PtCl_6 samples showed a larger change in sheet resistance than the K_2PtCl_4 samples. Furthermore, the presence of holes explains why the theoretical sheet resistance for a structurally identical

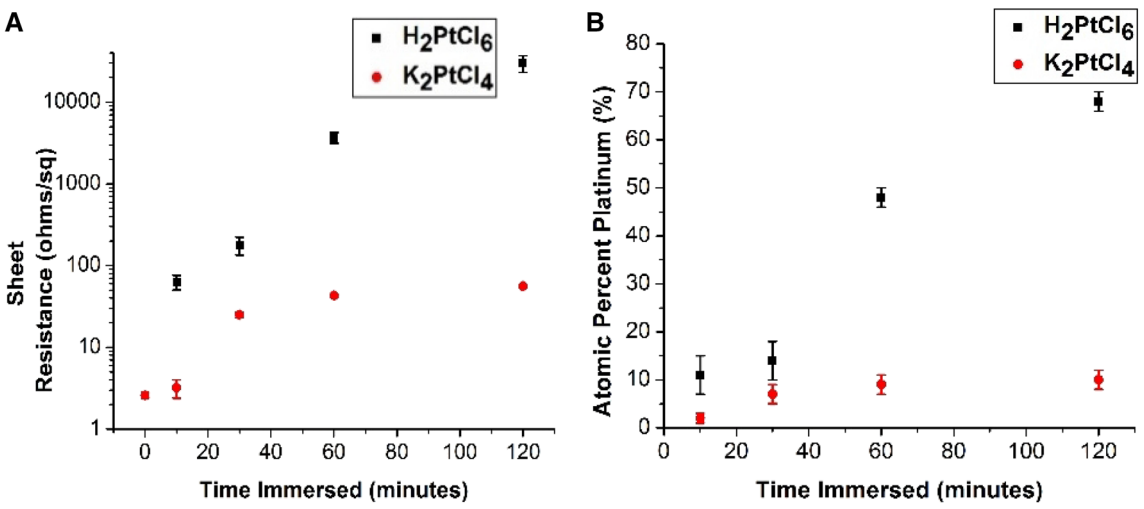

Fig. 1 Sheet resistances (**a**) and Pt percent compositions (**b**) of AgNWs on PET after immersion in 1.0 L of 100 µM H_2PtCl_6 (black) or K_2PtCl_4 (red) for 0, 10, 30, 60, and 120 min

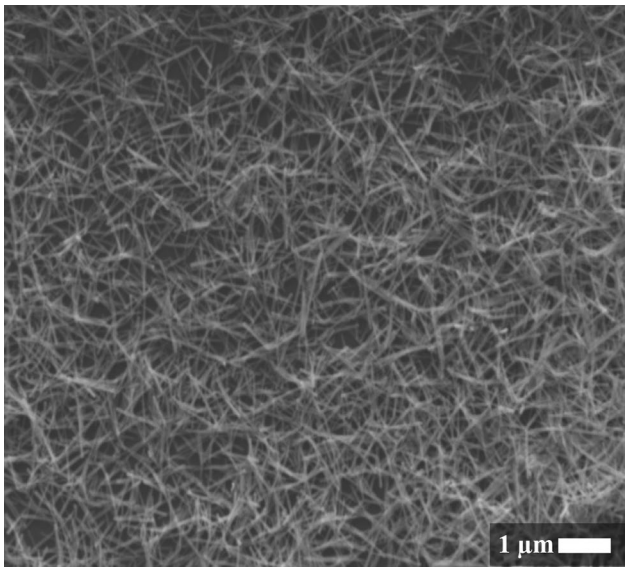

Fig. 2 Scanning electron microscope image of AgNWs on PET before galvanic displacement using Pt salts

PtNW array was surpassed. The gaps within the nanowire array decrease the number of interconnections among the nanowires and therefore make it more difficult for the materials to conduct electricity. The theoretical sheet resistance calculation for an identical PtNW sample did not account for these morphological changes and explains the larger than expected sheet resistances following immersion.

Increasing the concentration of the hexa/tetrachloroplatinate solutions resulted in larger changes in sheet resistances (Fig. 5a) and Pt percent compositions (Fig. 5b). For these experiments, the sample immersion time was kept constant at 30 min. We observed that the nanowire thin film delaminated from the PET substrate for the 1 mM and 10 mM H_2PtCl_6 solutions. This observation suggested that the rate of the displacement reaction under these high concentration conditions was very fast. Rapid galvanic displacement has been shown to result in nonuniform nucleation and rough growth profiles [34], which disrupts the contact points between the nanowires and the PET substrate, resulting in nanowire delamination.

The galvanic displacement reaction between Ag and $PtCl_6^{2-}/PtCl_4^{2-}$ through immersion is sensitive to the length of the immersion time (Fig. 1) and the concentration of the Pt bath (Fig. 5). The length of the immersion time is correlated to greater hole development, and higher Pt concentrations are associated with nanowire delamination. To gain further insight into the kinetics of the displacement reactions, we utilized UV–Vis spectroscopy. An aqueous solution of AgNWs shows two absorbance peaks at 350 nm and 420 nm (Fig. 6a, green), which correspond to the asymmetric transverse surface plasmons of the nanowires [35]. Both H_2PtCl_6 (Fig. 6a, black) and K_2PtCl_4 (Fig. 6a, red) exhibit significant absorbance at wavelengths

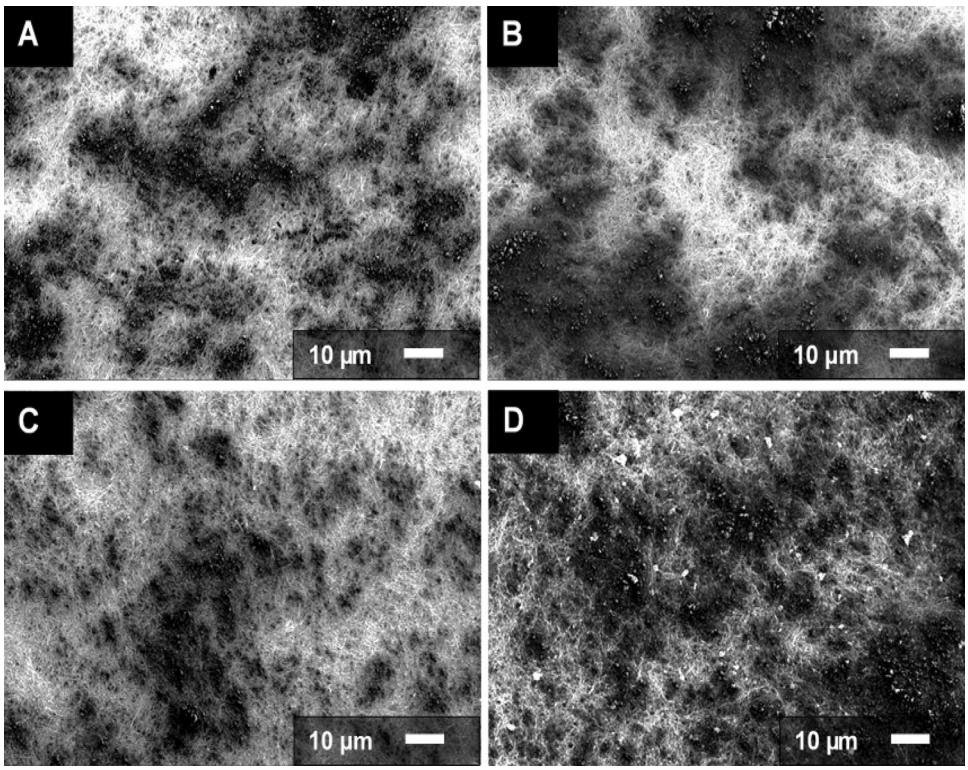

Fig. 3 Scanning electron microscope images of AgNWs on PET immersed in 1.0 L of 100 µM H_2PtCl_6 for 10 (**a**), 30 (**b**), 60 (**c**), and 120 (**d**) minutes

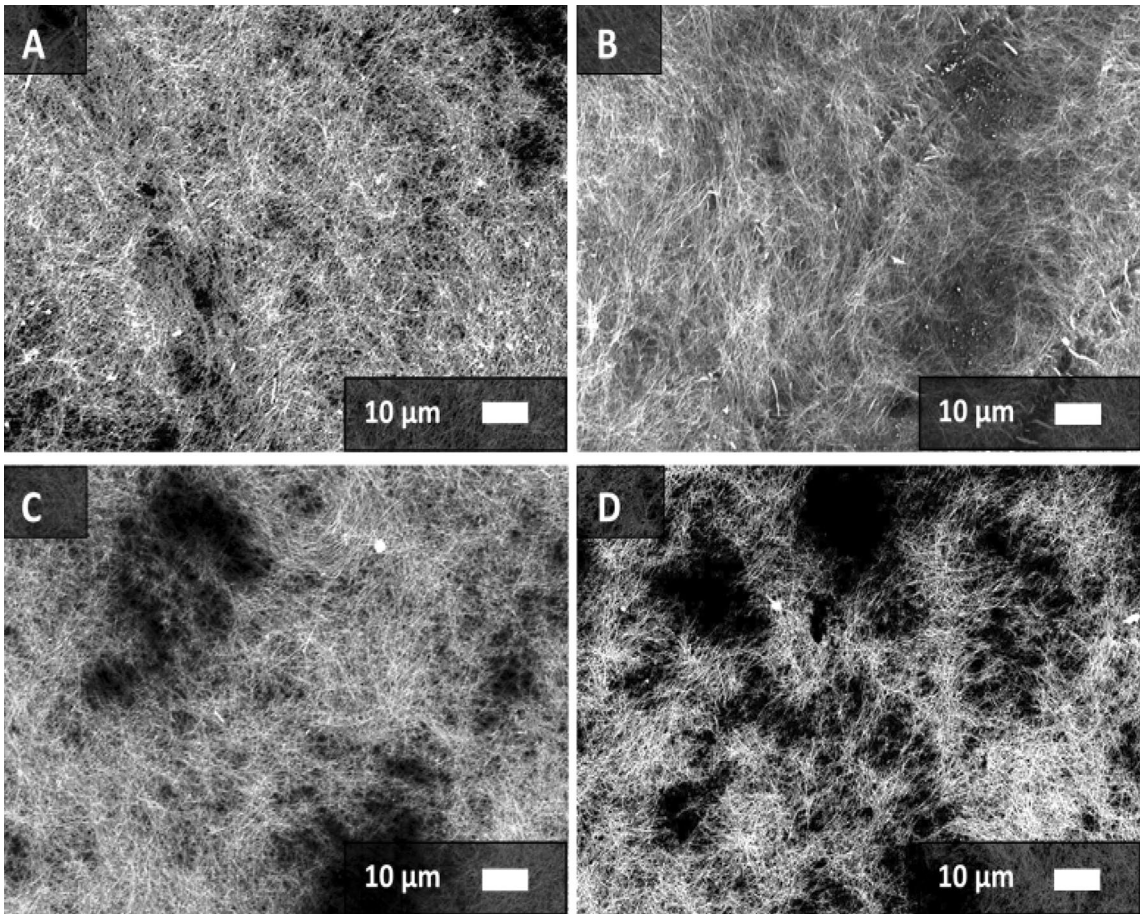

Fig. 4 Scanning electron microscope images of AgNWs on PET immersed in 1.0 L of 100 µM K_2PtCl_4 for 10 (**a**), 30 (**b**), 60 (**c**), and 120 (**d**) minutes

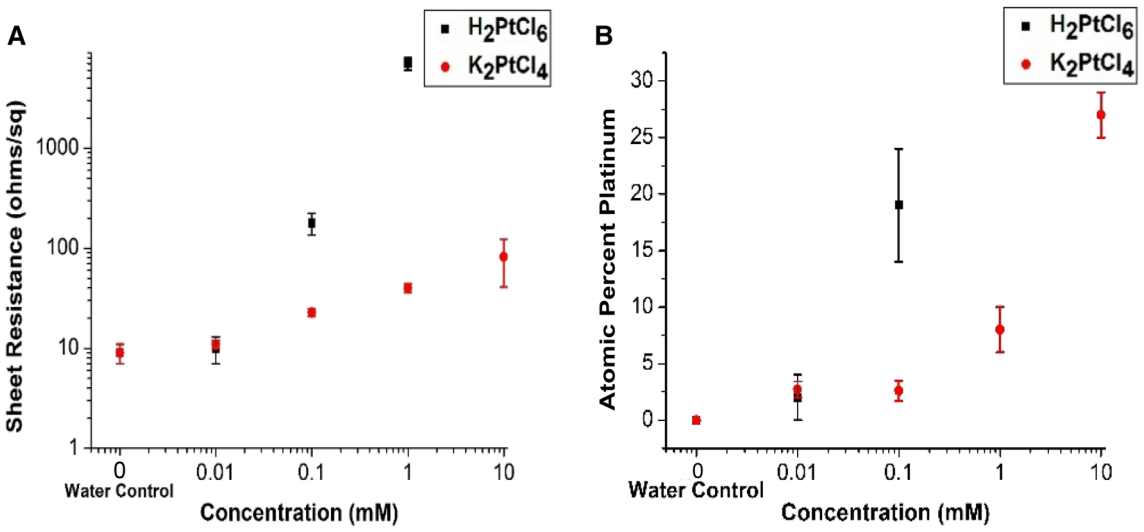

Fig. 5 Sheet resistances (**a**) and Pt percent compositions (**b**) of AgNWs on PET after a 30 min immersion in H_2O, 10 µM, 100 µM, 1 mM, and 10 mM H_2PtCl_6 (black) and K_2PtCl_4 (red)

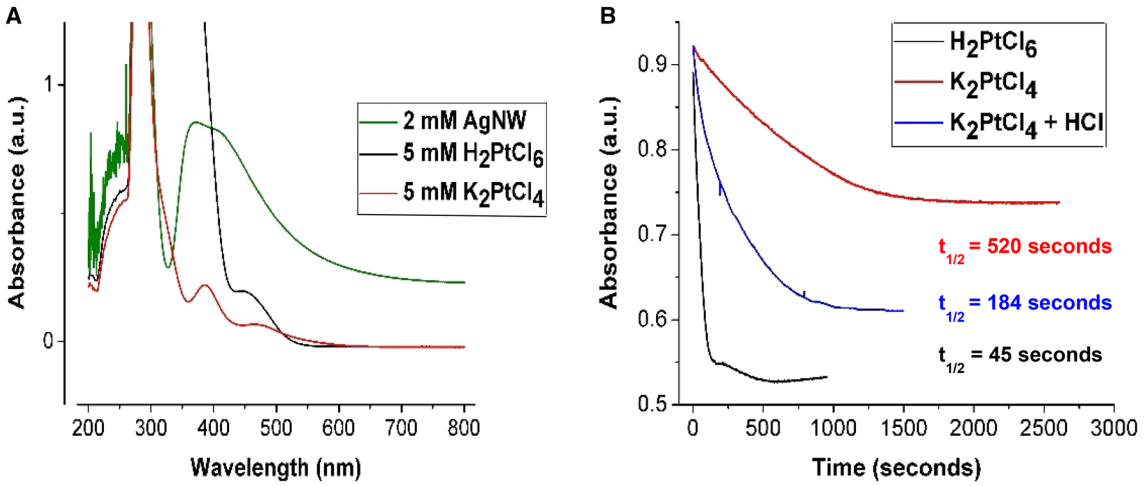

Fig. 6 UV–Vis spectra of 2 mM AgNWs (green), 5 mM H_2PtCl_6 (black), and 5 mM K_2PtCl_4 (red, **a**). Kinetic trace of 2 mM AgNWs at 420 nm in 5 mM H_2PtCl_6 (black), 5 mM K_2PtCl_4 (red), and 5 mM K_2PtCl_4 and 10 mM HCl (blue, **b**)

less than 400 nm, but do not absorb strongly at 420 nm. Therefore, we performed kinetic trace measurements of the AgNWs at 420 nm following the addition of H_2PtCl_6 or K_2PtCl_4 (Fig. 6b, black and red). In both cases, the absorbance at 420 nm decreases after the addition of the Pt reactant because the AgNWs are displaced during the reaction, thus causing a decrease in the absorbance of the AgNW plasmon mode. The time ($t_{1/2}$) it takes the absorbance to reach halfway between its maximum and minimum values differs substantially between the two cases. In particular, the $t_{1/2}$ values for H_2PtCl_6 and K_2PtCl_4 were determined to be 45 s and 520 s, respectively (Fig. 6b). These results are consistent with the greater thermodynamic favorability of $PtCl_6^{2-}$ to displace Ag, which arises from its more positive oxidation state (+4 vs. +2). However, in addition to the effects of differing Pt oxidation states, a confounding variable of different cations being present in solution exists ($H^+_{(aq)}$ vs. $K^+_{(aq)}$). Because K_2PtCl_6 is not very soluble in water and H_2PtCl_4 does not exist in the solid state (vide supra), we could not perform comparative experiments while only manipulating the Pt oxidation state. Therefore, to assess the effect of the $H^+_{(aq)}$ present in H_2PtCl_6, we performed an additional kinetic trace using K_2PtCl_4 with added HCl (Fig. 6b, blue). The addition of HCl decreased the $t_{1/2}$ for K_2PtCl_4 from 520 to 184 s. The accelerated kinetics in the presence of acid for K_2PtCl_4 is likely the result of acid catalyzing the displacement reaction via Ag etching. Importantly, however, the $t_{1/2}$ of H_2PtCl_6 is still significantly less than the $t_{1/2}$ of K_2PtCl_4 and HCl. These results demonstrate that the origin of the faster kinetics with H_2PtCl_6 as compared to K_2PtCl_4 is twofold. Both the acidity of H_2PtCl_6 and the thermodynamic favorability associated with its more positive Pt oxidation state result in faster displacement kinetics.

It is more thermodynamically favorable for $AgCl_{(s)}$ to form during the galvanic displacement reaction as opposed to $Ag^+_{(aq)}$ (compare Eqs. 1 and 3 to Eqs. 2 and 4). Our standard synthesis protocols include a wash with NH_4OH, which dissolves the unwanted $AgCl_{(s)}$ byproduct through the formation of soluble $Ag(NH_3)^{2+}$. We hypothesize that the location of $AgCl_{(s)}$ crystals within the nanowire array is reflective of nucleation and growth dynamics and explains the presence of holes in the Pt/AgNWs. Inspection of the Pt/AgNWs before and after the removal of $AgCl_{(s)}$ via SEM correlates the location of $AgCl_{(s)}$ crystals to thinning sections of the nanowire network (Fig. 7). For example, in one pair of SEM images taken at the same sample location, a large $AgCl_{(s)}$ crystal is present before NH_4OH immersion (Fig. 7a). This $AgCl_{(s)}$ crystal disappears after NH_4OH immersion and reveals a thinning segment of the Pt/AgNW array (Fig. 7b). The sites of initial Pt deposition result in the oxidation and ensuing nucleation of $Ag_{(S)}$ into $AgCl_{(s)}$. The first formed $AgCl_{(s)}$ crystals serve as seeds for future $AgCl_{(s)}$ growth and Pt deposition, as adding $AgCl_{(s)}$ to an existing crystal lattice is more favorable than producing new nucleation sites. In this manner, large $AgCl_{(s)}$ crystals form in isolated spots across the substrate, giving rise to concentrated patches of Pt deposition, resulting in gaps within the nanowire array yielding poor conductivity.

3.2 Synthesis of Pt/AgNWs with lower sheet resistances

Having elucidated the mechanism by which holes in the Pt/AgNWs form, we next sought to minimize their growth such that thin films with lower sheet resistances could be produced. Ideally, we would construct Pt/AgNWs using many cycles of short immersion times at low Pt

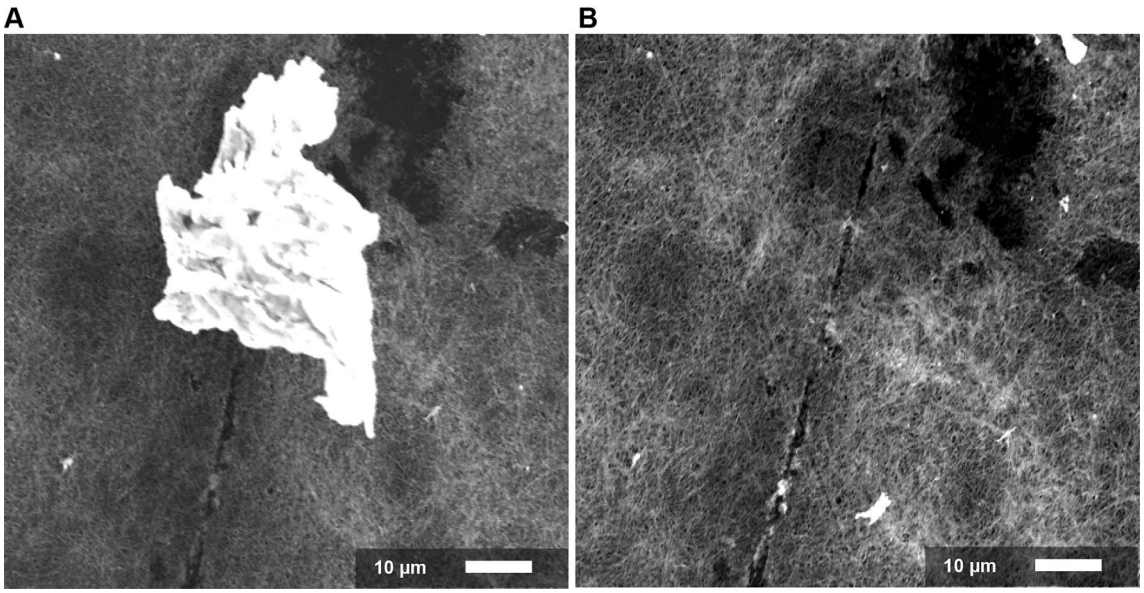

Fig. 7 Scanning electron microscopy images of AgNWs on PET at the same location after immersion in 20 mL of 10 mM K_2PtCl_4 before (**a**) and after 30 min in 100 mM $NH_4OH_{(aq)}$

bath concentrations. As our results above indicate, both of these parameters decrease the propensity of hole formation. In this paradigm, each cycle of Pt deposition and subsequent immersion in NH_4OH resets the nucleation sites for $AgCl_{(s)}$ formation. The establishment of new Pt/AgCl nucleation sites during each reaction cycle avoids the overconcentration of the displacement reaction in localized areas, which results in holes. With the desired short immersion times and low Pt bath concentrations, however, hundreds of cycles would be necessary to achieve appreciable conversion of Ag to Pt. In search of more practical reaction conditions, we sought to utilize faster reaction kinetics that still obviated hole formation. Towards this end, we first shortened the length of time of Pt immersion and increased the Pt bath concentration. We also increased the amount of time the Pt/AgNWs were immersed in NH_4OH to ensure the complete removal of nonconductive $AgCl_{(s)}$ precipitates. We focused these studies solely on K_2PtCl_4 because the faster reaction kinetics of H_2PtCl_6 result in both increased hole formation and nanowire delamination at high concentrations.

Immersion of AgNW samples in 10 mM K_2PtCl_4 for 1, 5, 10, 15, and 20 min showed a more gradual increase in sheet resistance (Fig. 8a) and atomic Pt percent composition (Fig. 8b) than previous experiments with longer immersion times at lesser concentrations. We did not immerse for times greater than 20 min because these longer immersion times resulted in nanowire delamination.

In an effort to further minimize the development of detrimental holes within the nanowire array, the thickness of the initial AgNWs was enlarged by increasing the number of spin coats on the PET substrate from 4 to 10. Previously it was observed that at concentrations greater than 1 mM for H_2PtCl_6 and 10 mM for K_2PtCl_4, delamination of the nanowires occurred from the substrate, presumably because the nanowires lost adhesion during rapid galvanic displacement. No loss of adhesion was observed with the 10 spin coated samples. However, if the number of spin coats of AgNWs was further increased, it is possible that the nanowires would become more fragile and prone to delamination from the underlying PET substrate. These samples were immersed under the same parameters as those in Fig. 8 and resulted in a more linear relationship between sheet resistance (Fig. 9a) and atomic Pt percentages (Fig. 9b) with smaller standard deviations among the samples. The more linear sheet resistance relationship observed is consistent with the fact that thicker AgNWs are slower to form nonconductive holes that completely penetrate the array. Nonetheless, the Pt percent compositions for the thicker Pt/AgNWs arrays are similar to the thinner arrays under the same conditions (Fig. 8b vs. Figure 9b). These results indicate that the galvanic displacement reaction is not limited by the amount of Ag present under these conditions.

To produce Pt/AgNWs with higher percent Pt compositions while maintaining low sheet resistances, we next controlled the nucleation dynamics of the displacement reaction using multiple cycles of 10-min Pt immersions. After one cycle of a 10-min Pt immersion, the average sheet resistance and atomic Pt percent composition were ~ 11 Ω/sq and ~ 12% Pt, respectively. Repeating these reaction conditions for a total of 2, 3, or 4 immersion cycles

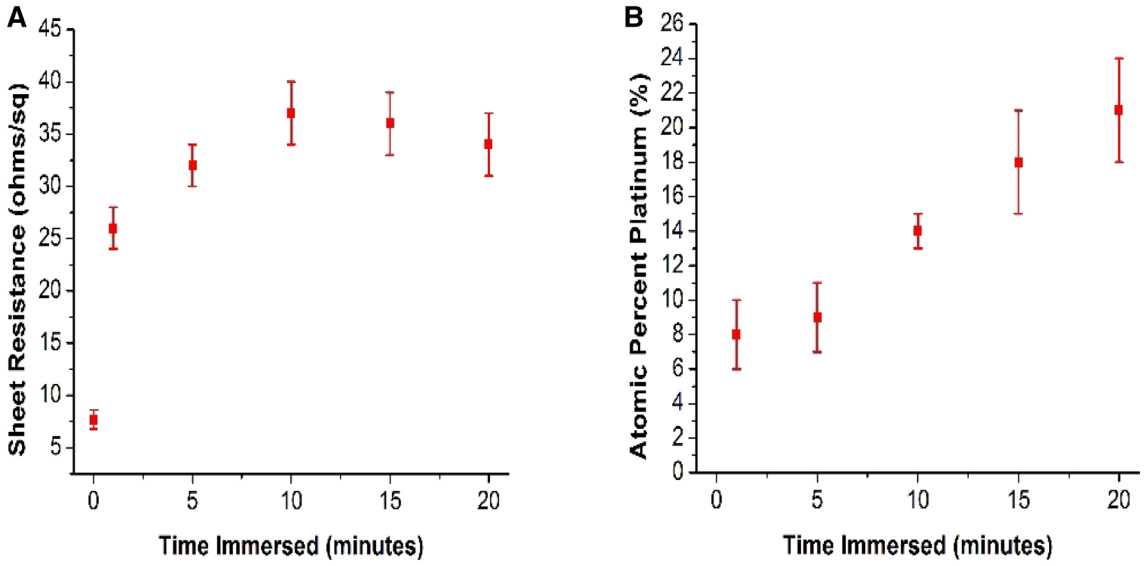

Fig. 8 Sheet resistances (**a**) and Pt percent compositions (**b**) of AgNWs on PET formed using 4 spin-coating cycles after immersion in 20 mL of 10 mM K_2PtCl_4 for 0, 1, 5, 10, 15, or 20 min

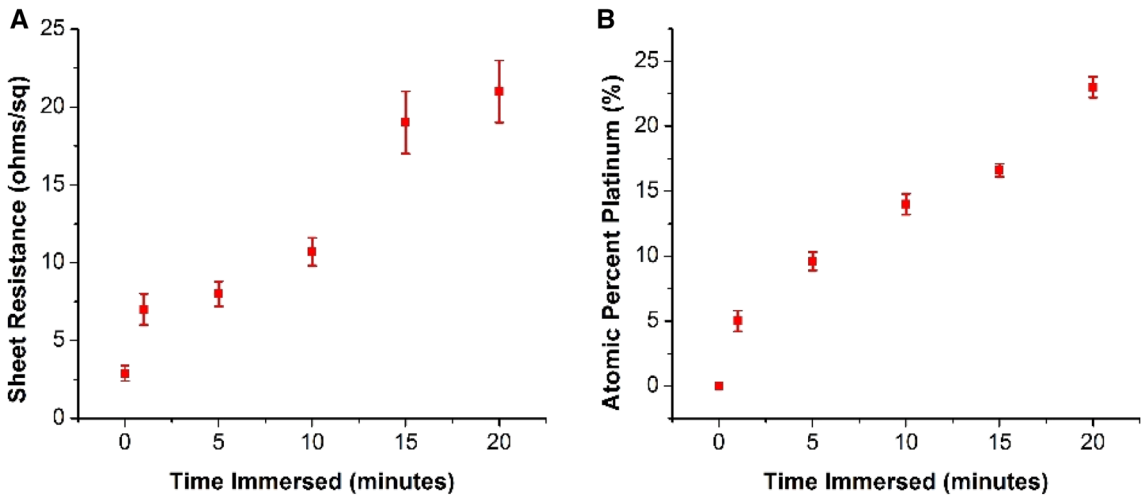

Fig. 9 Sheet resistances (**a**) and Pt percent compositions (**b**) of AgNWs on PET formed using 10 spin-coating cycles after immersion in 20 mL of 10 mM K_2PtCl_4 for 0, 1, 5, 10, 15, or 20 min

(each cycle consisted of 10 min of Pt immersion followed by a 30-min immersion in 100 mM NH_4_OH) resulted in a progressive increase in sheet resistance (Fig. 10a) and atomic Pt percent composition (Fig. 10b, red points) as determined by EDX. The Pt/AgNW samples produced using 4 immersion cycles of 10 min possessed an average sheet resistance of ~ 34 Ω/sq and a Pt percent composition of ~ 42%. The Pt percent compositions of these samples were confirmed with ICP-MS (Fig. 10b, black points). Among all of the conditions studied in this manuscript, these parameters yielded Pt/AgNW arrays with the highest ratio of Pt percent composition to sheet resistance. SEM images indicate that the diameters of the nanowires increased progressively from their original 25–35 nm diameters to 30–60 nm after the successive 10-min immersions (Fig. 11). These results indicate that Pt deposition thickens the AgNWs proportional to the number of 10-min immersions. Importantly, in all cases, the nanowires, which are several microns long, maintain their high aspect ratios (150–500) after the galvanic displacement reactions with Pt.

Our efforts to further increase Pt percent composition with further immersion cycles did not yield Pt/AgNWs with Pt compositions greater than 40%. One possibility is that

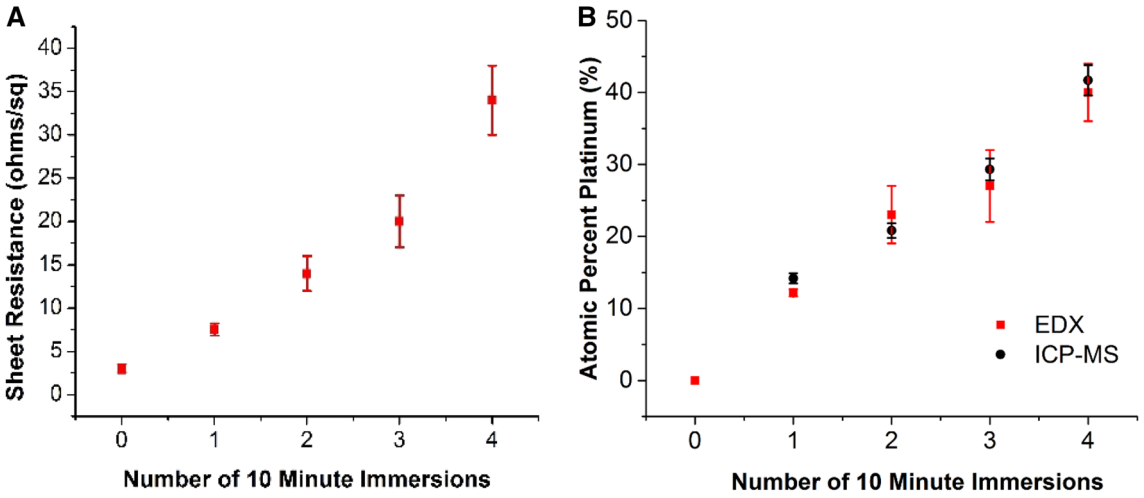

Fig. 10 Sheet resistances (**a**) and Pt percent compositions (**b**) of AgNWs as determined by EDX (red) and ICP-MS (black) on PET formed using 10 spin-coating cycles after 1, 2, 3, and 4 ten-minute immersions in 20 mL of 10 mM K_2PtCl_4

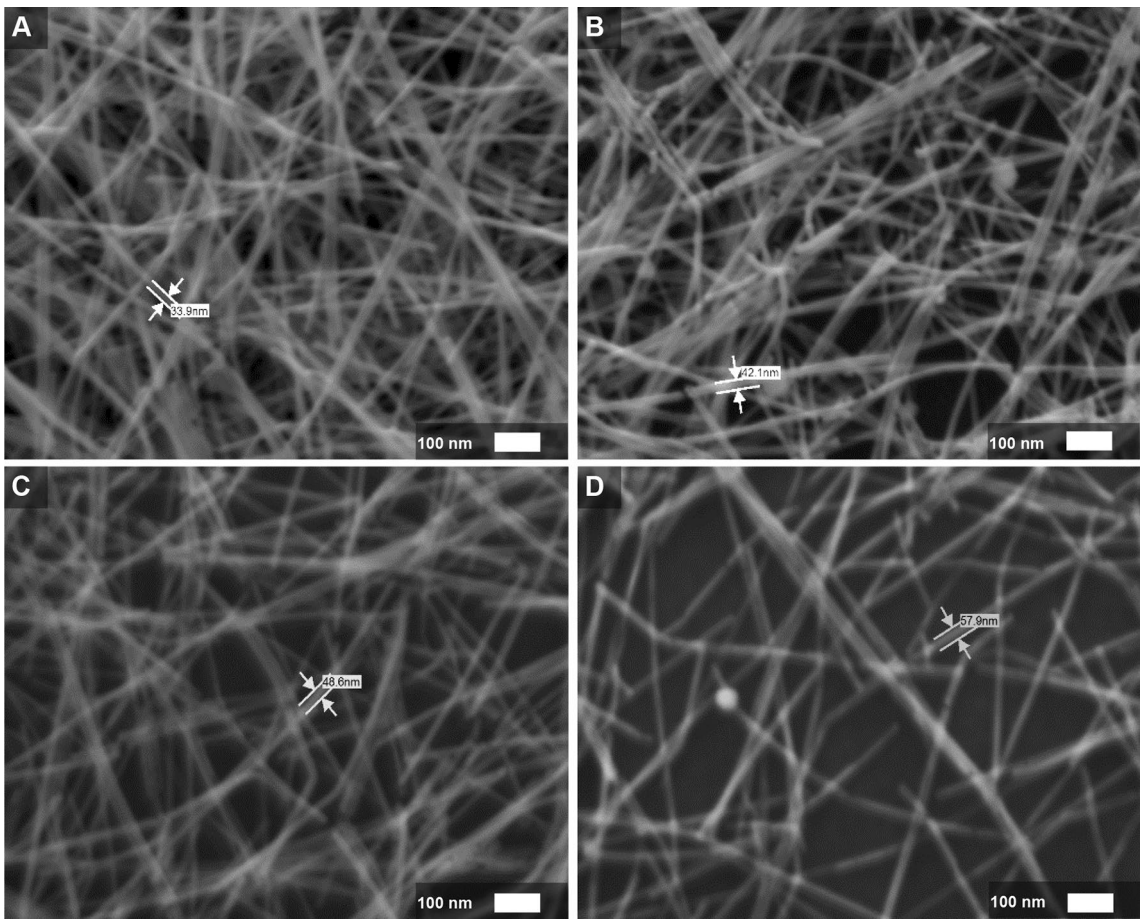

Fig. 11 Scanning electron microscope images of ~ 10% atomic Pt/AgNWs (**a**), ~ 20% atomic Pt/AgNWs (**b**), ~ 30% atomic Pt/AgNWs (**c**), and ~ 40% atomic Pt/AgNWs (**d**) on PET

the concentration of the Pt bath decreased to a point at which the galvanic displacement kinetics are very slow. However, experiments immersing the 40% Pt/AgNW samples in fresh Pt solutions also did not increase the Pt percent composition and only marginally affected sheet resistances. Furthermore, soaking the Pt/AgNWs in nitric acid, which selectively dissolves Ag, did not significantly change the Pt percent composition. These results suggest that the Pt deposition in the 40% Pt/AgNW samples fully encapsulated the AgNW cores, thus preventing further galvanic displacement from occurring.

3.3 Pt/AgNWs as electrodes for reversible metal electrodeposition

If the Pt/AgNWs consist of AgNWs fully encapsulated by Pt shells, one potential application of transparent versions of these materials is in dynamic windows based on reversible metal electrodeposition. Previous studies on metal-based dynamic windows have shown that performing reversible electrodeposition of Bi and Cu from an acidic electrolyte results in the slow deterioration of the transparent ITO electrodes as a result of the acid etching the ITO [36]. The inertness of Pt would allow Pt-coated AgNWs to withstand both the acidity of these electrolytes and provide the electrochemical window needed for both the metal electrodeposition and stripping processes. We therefore performed cyclic voltammetry in a typical Bi–Cu electrolyte for reversible metal electrodeposition. This experiment is not only a gauge of the applicability of Pt/AgNWs for dynamic window applications, but it is also a further test of the hypothesis that the nanowires consist of AgNWs encapsulated by Pt shells. Cyclic voltammograms from + 0.8 to − 0.6 V (vs. Ag/AgCl) in an acidic (pH 2) Bi–Cu electrolyte show that a control experiment with a pure AgNW electrode exhibits metal electrodeposition and stripping features, but deteriorates after ~ 6 cycles due to Ag dissolution during the metal stripping processes (Fig. 12a). In contrast, the current density of an electrode with Pt/AgNWs decreases from cycle 1 to 20, but maintains a relatively constant current density after cycle 20 (Fig. 12b). To better visualize the relative rates of degradation, the

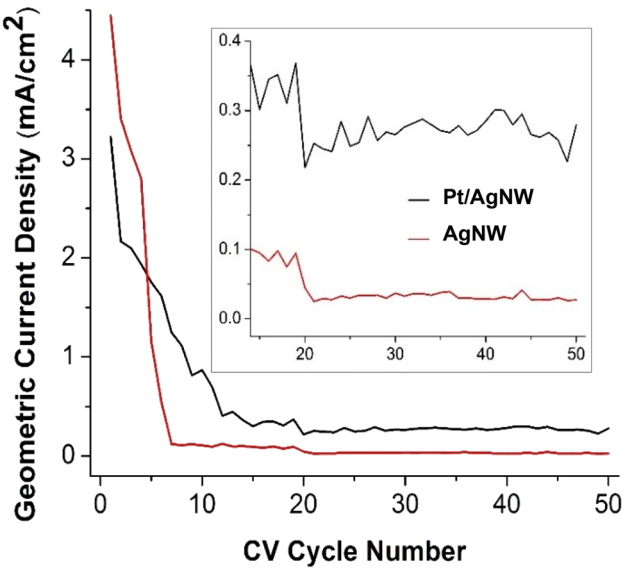

Fig. 13 Current density at − 0.6 V for Pt/AgNWs (black) and AgNWs (red) on PET during successive CV cycles of reversible Bi and Cu electrodeposition

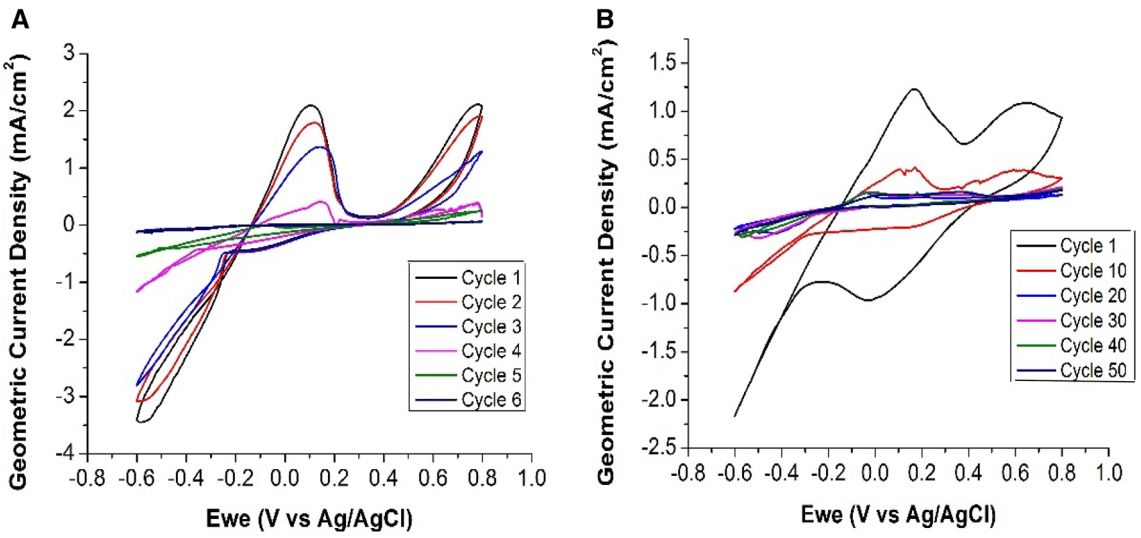

Fig. 12 Cyclic voltammograms in terms of geometric current density (mA/cm^2) at 10 mV/s for unmodified AgNWs on PET (**a**) and modified Pt/AgNWs on PET (**b**)

current density of each sample at − 0.6 V was compared for each cycle (Fig. 13). While the Pt/AgNW sample (Fig. 13, black) possessed a current density of ~ 0.25 mA/cm^2 after 20 cycles, the AgNW sample (Fig. 13, red) exhibited a negligible current density after cycle 20. These results indicate that the Pt/AgNWs are much more stable than the AgNWs towards electrodissolution during the metal stripping processes and suggests that the electrochemically more reactive AgNWs are fairly well encapsulated by Pt shells in the Pt/AgNWs. The initial decay of current density during the first 20 cycles, however, does indicate some instability of the Pt/AgNWs during the Bi and Cu electrodeposition and stripping reactions. This decay could be due to imperfect encapsulation of the AgNWs by the Pt shells. However, given the inertness of the Pt/AgNWs towards Pt salts and nitric acid, it is more likely that a larger contribution to the initial decay of current density is physical delamination of nanowires caused by stress and strain buildup during reversible metal electrodeposition. Regardless, the results point towards the potential application of Pt/AgNWs in reactive reversible metal electrodeposition electrolytes.

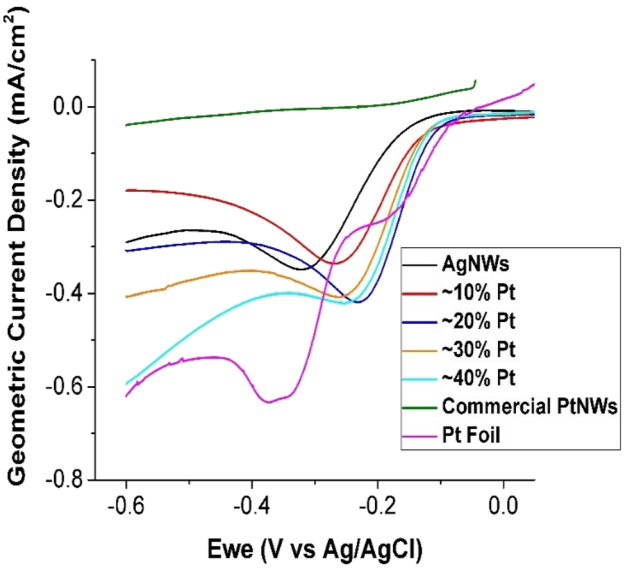

Fig. 14 ORR polarization curves in 0.1 M KOH in terms of geometric current density (mA/cm^2) at 10 mV/s for the synthesized bimetallic Pt/AgNW electrodes with varying Pt compositions (red, blue, orange, cyan), AgNWs (black), commercial PtNWs (green), and Pt foil (pink)

3.4 Pt/AgNWs as oxygen reduction electrocatalysts

Pt is the most common oxygen reduction reaction (ORR) catalyst in the cathode of commercial proton exchange membrane fuel cells due to its low overpotential and good durability [37]. Because of the high cost of Pt, Pt nanostructures are used to increase catalyst surface area and decrease Pt loadings. Ag is also a promising ORR catalyst, but Ag dissolution occurs in acid, rendering it unstable in proton exchange membrane fuel cell electrolytes. Although proton exchange membrane fuel cells are currently the most successful for many applications, there is increasing interest in anion exchange membrane fuel cells that function in alkaline environments [38]. Both Ag and Pt are promising candidates for the ORR in high pH electrolytes. We therefore hypothesized that the Ag/Pt NWs described in this work would be highly active ORR catalysts in basic solutions.

Samples produced via 1, 2, 3, and 4 cycles of 10-min immersions in 10 mM K_2PtCl_4 were evaluated as electrocatalysts for the oxygen reduction reaction (ORR) in O_2-sparged 0.1 M KOH. Their catalytic activity was compared to AgNWs, commercially obtained PtNWs, and Pt foil. ORR linear sweep voltammograms for these various catalysts are shown in Fig. 14 in terms of their geometric current density. The ORR onset potential, defined here as the voltage at which the current density reaches 10% of its peak current density, for the AgNWs occurs at about − 0.17 V vs. Ag/AgCl (Fig. 14, black). In contrast, the onset potential for Pt foil occurs at about − 0.10 V (Fig. 14, pink), indicating that Pt possesses ~ 70 mV less onset overpotential for the ORR. These values are similar to previous literature results studying Ag and Pt ORR catalysts under alkaline conditions [39]. The onset potentials for the 10–40% Pt/AgNWs vary between − 0.11 V and − 0.14 V (Fig. 14, red, blue, orange, and cyan), indicating that the onset overpotentials for these bimetallic catalysts are in between those of the monometallic Pt and Ag catalysts.

In terms of geometric current density, the commercial PtNWs showed minimal ORR activity (Fig. 14, green) because the concentration of nanowires on the PET is much less than our synthesized Pt/AgNWs. To more accurately compare the activities of the commercial PtNWs with the Pt/AgNWs, we normalized the current of the polarization curves per mass of Pt (Fig. 15a). These polarization curves are the most relevant for assessing the usefulness of Pt-based ORR catalysts because they account for the electrocatalytic activity per amount of Pt, which is 50–60 times more expensive than Ag [40, 41]. On a per mass of Pt basis, the bimetallic Pt/AgNWs prepared via galvanic displacement significantly outperformed pure PtNWs and Pt foil. Furthermore, there is a trend in the peak current densities of 10–40% Pt/Ag NW catalysts in which 20% Pt > 10% ~ 30% Pt > 40% Pt (Fig. 15b). The highest peak current density on a mass Pt basis obtained for the 20% Pt NWs can be rationalized as follows. 100% PtNWs are intrinsically the most active catalysts, but because they contain pure Pt, their current density on a per Pt mass basis is poor. On the other hand, 100% AgNWs do not use any expensive Pt, but are intrinsically less electrochemically

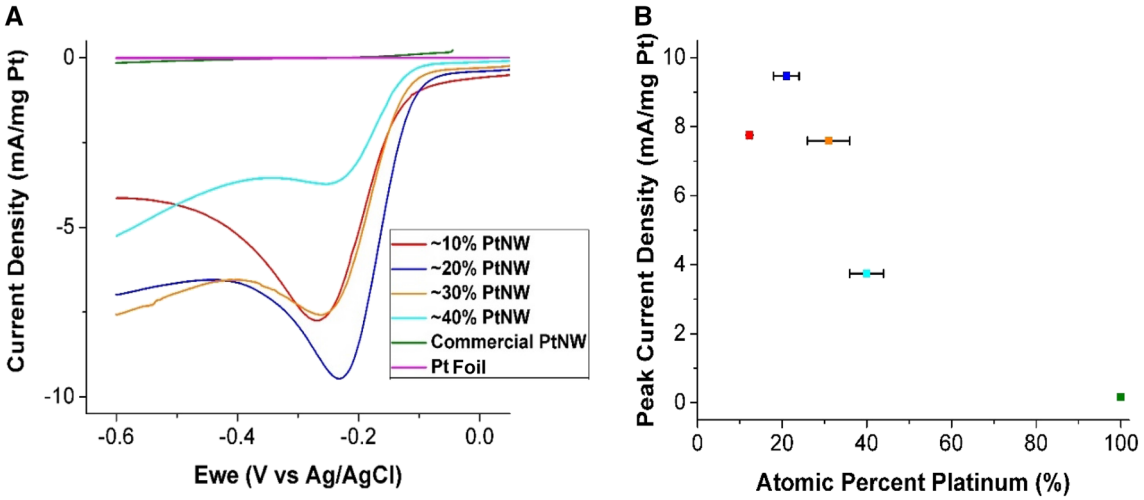

Fig. 15 ORR polarization curves (**a**) in terms of current density normalized to mass of Pt (mA/mg Pt) at 10 mV/s in 0.1 M KOH for the synthesized bimetallic Pt/AgNW electrodes with varying Pt compositions (red, blue, orange, cyan), commercial PtNWs (green), and Pt foil (pink). A plot of the peak current densities obtained from **a** versus their respective atomic percentages of Pt demonstrates that the 20% Pt sample is the most electrochemically active per amount of Pt present (**b**)

active. The bimetallic Pt/AgNW array catalysts strike a balance between these two competing factors, with the 20% Pt sample being the most electrochemically active per Pt mass (Fig. 15b, blue). Taken together, these results demonstrate that Pt/AgNWs are promising candidates for ORR catalysts under alkaline conditions that use minimal amounts of Pt.

4 Conclusions

Bimetallic electrodes of Pt/AgNWs were prepared through an immersive galvanic displacement method in which spin-coated AgNWs are displaced by $PtCl_6^{2-}$ and $PtCl_4^{2-}$ ions. The galvanic displacement is sensitive to time of immersion and Pt concentration, which dramatically affect the conductivity of the electrodes. Shorter immersion times at higher concentrations of $PtCl_4^{2-}$ proved to be promising parameters to yield more conductive electrodes with controllable amounts of Pt. This method provides an array of conductive Pt nanomaterials that employs Pt to a better degree than commercial PtNWs for ORR. The Pt/AgNWs also serve as relatively stable platforms for reversible metal electrodeposition. With continued development, these bimetallic nanowires could find applications in a variety of other renewable energy devices.

Acknowledgements This research was funded by Research and Innovation at the University of Nevada, Reno (UNR). We also acknowledge the Share Instrumentation Laboratory in the Department of Chemistry at UNR. SEM–EDX analysis was performed in the Mackay Microbeam Laboratory at UNR, and we thank J. Desormeau for his kind assistance.

Compliance with ethical standards

Conflict of interest On behalf of all authors, the corresponding author states that there is no conflict of interest.

References

1. Tyler TP, Brock RE, Karmel HJ, Marks TJ, Hersam MC (2011) Electronically monodisperse single-walled carbon nanotube thin films as transparent conducting anodes in organic photovoltaic devices. Adv Energy Mater 1:785–791
2. Kymakis E, Stratakis E, Koudoumas E, Fotakis C (2011) Plasmonic organic photovoltaic devices on transparent carbon nanotube films. IEEE Trans Electron Dev 58:860–864
3. Steirer KX, Chesin JP, Widjonarko NE, Berry JJ, Miedaner A, Ginley DS, Olson DC (2010) Solution Deposited NiO thin-films as hole transport layers in organic photovolaics. Org Electron 8:1414–1418
4. Wilson MS, Gottesfeld S (1992) Thin-film catalyst layers for polymer electrolyte fuel cell electrodes. J Appl Electrochem 22:1–7
5. Han GB, Lee JN, Choi JW, Park JK (2011) Tris(pentafluorophenyl) borane as an electrolyte additive for high performance silicon thin film electrodes in lithium ion batteries. Electrochim Acta 24:8997–9003
6. Zhou YN, Xue MZ, Fu ZW (2013) Nanostructured thin film electrodes for lithium storage and all-solid-state thin-film lithium batteries. J Power Sources 15:310–332
7. Islam SM, Hernandez TS, McGehee MD, Barile CJ (2019) Hybrid dynamic windows using reversible metal electrodeposition and ion insertion. Nat Energy 4:223–229
8. Liu Y, Zhou H, Cheng R, Yu W, Huang Y, Duan X (2014) Highly flexible electronics from scalable vertical thin film transistors. Nano Lett. 14:1413–1418
9. From touch displays to the surface: a brief history of touchscreen technology. https://arstechnica.com/gadgets/2013/04/from-touch-displays-to-the-surface-a-brief-history-of-touchscreen-technology/. Accessed 22 Jan 2020

10. Cairns DR, Witteli RP, Sparacin DK, Sachsman SM, Paine DC, Crawford GP, Newton RR (2000) Mechanical reliability of indium tin oxide electrodes on polymer substrates for lightweight flexible displays. Appl Phys Lett 76:1425
11. Tahar RBH, Ban T, Ohya Y, Takahashi Y (2001) Effect of processing parameters on physical properties of cadmium stannate thin films prepared by a dip-coating technique. J Am Ceram Soc 84:85–91
12. Espinosa N, Garcia-Valverde R, Urbina A, Krebs FC (2011) A life cycle analysis of polymer solar cell modules prepared using roll-to-roll methods under ambient conditions. Sol Energy Mater Sol Cells 95:1293–1302
13. Nguyen WH, Barile CJ, McGehee MD (2016) Small molecular anchored to mesoporous ITO for high-contrast black electrochromics. J Phys Chem C 120:26336–26341
14. van de Lagemaat J, Barnes TM, Rumbles G, Shaheen SE, Coutts TJ (2006) Organic solar cells with carbon nanotubes replacing In2 O3: Sn as the transparent electrode. Appl Phys Lett 88:233503
15. Han TH, Lee Y, Choi MR, Woo SH, Bae SH, Hong BH, Ahn JH, Lee TW (2012) Extremely efficient flexible organic light-emitting diodes with modified graphene anode. Nat Photonics 6:105–110
16. Tokuno T, Nogi M, Karakawa M, Jiu J, Nge TT, Aso Y, Suganuma K (2011) Fabrication of silver nanowire transparent electrodes at room temperature. Nano Res 4:1215–1222
17. Liu CH, Yu X (2011) Silver nanowire-based transparent, flexible, and conductive thin film. Nanoscale Res Lett 6:1–8
18. Na SI, Kim SS, Jo J, Kim DY (2008) Efficient and flexible ITO-free organic solar cells using highly conductive polymer anodes. Adv Mater 20:4061–4067
19. Xia X, Yang B, Zhang X, Zhou C (2015) Enhanced film conductance of silver nanowire-based flexible transparent & conductive networks by bending. Mater Res Express 2:075009
20. Sun J, Zhou W, Yang H, Zhen X, Ma L, Williams D, Sun X, Lang MF (2018) Highly transparent and flexible circuits through patterning silver nanowires into microfluidic channels. Chem Commun 54:4923–4926
21. Madaria AR, Kumar A, Zhou C (2011) Large scale, highly conductive and patterned transparent films of silver nanowires on arbitrary substrates and their application in touch screens. Nanotech 22:245201
22. Abedin SZE, Endres F (2009) Electrodeposition of nanocrystalline silver films and nanowires from the ionic liquid 1-ethyl-3-methylimidazolium trifluoromethylsulfonate. Electrochim Acta 54:5673–5677
23. Hu L, Kim HS, Lee JY, Peumans P, Cui Y (2010) Scalable coating and properties of transparent, flexible, silver nanowire electrodes. ACS Nano 4:2955–2963
24. Mayousse C, Celle C, Fraczkiewicz A, Simonato JP (2015) Stability of silver nanowire based electrodes under environmental and electrical stress. Nanoscale 7:2107–2115
25. Elechiguerra JL, Larios-Lopez L, Lui C, Garcia-Gutierrez D, Camacho-Bragada A, Yacaman MJ (2005) Corrosion at the nanoscale: the case of silver nanowires and nanoparticles. Chem Mater 17:6042–6052
26. Chung HT, Won JH, Zelenay P (2013) Active and stable carbon nanotube/nanoparticle composite electrocatalyst for oxygen reduction. Nat Commun 4:1922
27. Tao F, Dag S, Wang LW, Liu Z, Butcher DR, Bluhm H, Salmeron M, Somorjai GA (2010) Break-up of stepped platinum catalyst surfaces by high CO coverage. Science 327:850–853
28. Lu YC, Xu Z, Gasteiger HA, Chen S, Schifferli KH, Shao-Horn Y (2010) Platinum–gold nanoparticles: a highly active bifunctional electrocatalyst for rechargeable lithium–air batteries. J Am Chem Soc 132:12170–12171
29. Wang B, Wang Y, Park J, Ahn H, Wang G (2011) *In Situ* synthesis of Co_3O_4/graphene nanocomposite material for lithium–ion batteries and supercapacitors with high capacity and supercapacitance. J Alloys Compd 509:7778–7783
30. Alia SM, Zhang G, Kisailus D, Li D, Gu S, Jensen K, Yan Y (2010) Porous platinum nanotubes for oxygen reduction and methanol oxidation reactions. Adv Func Mater 20:3742–3746
31. Kim KT, Jin SH, Chang SC, Park DS (2013) Green synthesis of platinum nanoparticles by electroreduction of a K_2PtCl_6 solid-state precursor and its electrocatalytic effects on H_2O_2 reduction. Bull Korean Chem Soc 34:3835–3839
32. Atomistry. http://platinum.atomistry.com/tetrachlor~platinous_acid.html. Accessed 17 Feb 2020
33. Serway RA, Jewett JW (1998) Principles of physics, 2nd edn. Harcourt College Pub, San Diego, p 602
34. Guo S, Dong S, Wang EA (2008) General method for the rapid synthesis of hollow metallic or bimetallic nanoelectrocatalysts with urchinlike morphology. Chem Eur J 14:4689–4695
35. Luu QN, Doorn JM, Berry MT, Jiang C, Lin C, May PS (2011) Preparation and optical properties of silver nanowires and silver-nanowire thin films. J Colloid Interface Sci 356:151–158
36. Miller DD, Li JY, Islam SM, Jeanetta JF, Barile CJ (2020) Aqueous alkalie electrolytes for dynamic windows based on reversible metal electrodeposition with improved durability. J Mater Chem C 8:1826–1834
37. Yang S, Kim J, Tak YJ, Soon A, Lee H (2015) Single-atom catalyst of platinum supported on titanium nitride for selective electrochemical reactions. Angew Chem Int Ed 55:2058–2062
38. Dekel DR (2018) Review of cell performance in anion exchange membrane fuel cells. J Power Sources 375:158–169
39. Erikson H, Sarapuu A, Tammeveski K (2018) Oxygen reduction on silver catalysts in alkaline media: a minireview. ChemElectroChem 6:73–86
40. JM Bullion. https://www.jmbullion.com/charts/silver-prices/. Accessed 14 Feb 2020
41. JM Bullion. https://www.jmbullion.com/charts/platinum-price/. Accessed 14 Feb 2020